Role of in situ-excited planetary waves in polar vortex splitting during the 2002 Southern Hemisphere sudden stratospheric warming event

- 4 Ji-Hee Yoo¹ and Hye-Yeong Chun¹
- ⁵ Department of Atmospheric Sciences, Yonsei University, Seoul, 03722, South Korea
- 6 Correspondence to: Hye-Yeong Chun (chunhy@yonsei.ac.kr)
- **Abstract.** On 25 September 2002, the Southern Hemisphere experienced its first and only major sudden stratospheric 8 warming (SSW02) since routine upper-atmosphere observations commenced in 1957. This event was marked by a sudden 9 splitting of the polar vortex. While previous studies focused on tropospheric waves and vortex preconditioning, the role of in 10 situ-excited planetary waves (PWs) remains unexplored. The current study addressed this gap by examining the impact of in situ-generated PWs on SSW02. As the onset approached, the displaced polar vortex elongated and split into two. The 11 explosive amplification of zonal wavenumber (ZWN) 2 PWs (PW2) at 10 hPa was driven not only by upward-propagating 12 13 PW2 from below but also by westward- and downward-propagating PW2 excited in the mid-to-upper stratosphere. This 14 spontaneous PW2 generation was associated with barotropic-baroclinic instability, triggered by easterlies descending from 15 the polar lower mesosphere. An unusual poleward shift of the polar vortex facilitated the development of easterlies by directing ZWN1 PWs (PW1) into the polar stratosphere, where they deposited strong westward momentum. This poleward 16 displacement was attributed to anomalous easterlies in the equatorial upper stratosphere. PW2 amplification via instability 17 occurred through two mechanisms: (i) PW1 breaking generated smaller-scale waves through energy cascading while 18 19 inducing instability that amplified these smaller-scale waves, and (ii) over-reflection of upward-propagating PW2. Nonlinear 20 wave-wave interaction drove early wave generation, while the latter played a role near the onset. Instability-driven wave 21 growth and equatorial easterlies in the upper stratosphere also appear in other vortex-splitting SSWs, suggesting their 22 broader significance in SSW dynamics.

2324

25

26

1 Introduction

- 27 On 25 September 2002, the first major sudden stratospheric warming (SSW) event (hereafter referred to as SSW02) was
- 28 recorded in the Southern Hemisphere (SH), marking an unprecedented occurrence in Antarctic stratospheric observations
- 29 since 1957. Although minor warmings have occasionally been observed in the SH, a major warming event characterized by

the complete breakdown of the polar vortex during spring has only been documented in this instance. The rarity of SSW in the SH has been attributed to several factors, including the less mountainous terrain; weak longitudinal land–sea contrasts; and the nearly zonally symmetric, cold, elevated Antarctic surface (Gray et al., 2005). These factors collectively suppress SSW in the SH by weakening planetary wave (PW) forcing and strengthening the polar-night jet (PNJ). However, SSW02 was distinguished by a record-breaking weakening of the PNJ and extremely high temperatures, both of which remain unparalleled in the SH climate.

Notably, SSW02, the first observed major SSW event in the SH, was of the split type, a phenomenon far less common than displacement-type warmings in the Northern Hemisphere (NH, Charlton et al., 2005). The vortex split significantly impacted the typically quiescent Antarctic ozone hole, causing it to divide into two separate regions (Allen et al., 2003; Baldwin, 2003). Using a mechanistic model, Manney et al. (2005) demonstrated that the vortex split could be simulated exclusively with zonal wavenumber (ZWN) 2 waves at the 100 hPa pressure level without requiring vortex preconditioning. This finding suggests that anomalously strong wave forcing in the lower stratosphere was the primary driver of the major warming. Krüger et al. (2005) attributed the intense stratospheric wave forcing to unusually strong tropospheric wave pulses, collectively formed by the quasi-stationary PWs of ZWNs 1–3. However, unlike Manney et al. (2005), they emphasized that the substantial weakening of the PNJ during early winter (July–August 2002) served as a crucial preconditioning factor that significantly amplified the upward propagation of tropospheric waves into the stratosphere (see also Baldwin, 2003).

Newman and Nash (2005) observed that the PNJ was preconditioned to not only weaken significantly but also to shift unusually poleward, thereby directing tropospheric waves toward the pole across a broad altitude range into the middle stratosphere. This abnormally poleward-shifted vortex structure was accompanied by the westerly quasi-biennial oscillation (QBO) in the lower stratosphere (30–50 hPa) and anomalous easterlies in the equatorial upper stratosphere (1–10 hPa), where the semiannual oscillation (SAO) dominates (Gray et al., 2005; Newman and Nash, 2005). Given that the westerly QBO is generally unfavorable for initiating SSWs (Holton and Tan, 1982) and that SSWs typically begin with wind reversal in the upper stratosphere and lower mesosphere, Gray et al. (2005) examined the influence of anomalous equatorial easterlies in the upper stratosphere on the onset of SSW02. Their analysis revealed that this wind structure could have contributed to triggering SSW02 by confining equatorward-propagating PWs to the pole during early and midwinter. Meanwhile, Charlton et al. (2005) emphasized that the vortex split dynamics involved complex nonlinear interactions within the coupled troposphere–stratosphere system, suggesting that the conventional framework of lower atmospheric forcing may be insufficient to comprehensively account for this event.

While previous research on SSW02 primarily focused on the role of tropospheric waves and vortex preconditioning in directing these waves toward the polar stratosphere, recent studies on SSWs in the NH have increasingly highlighted the role of in situ-excited PWs within the stratosphere or mesosphere. Regarding the split SSW event in January 2009, Song et al.

(2020) suggested that the eastward-propagating PWs of ZWN2 (PW2) excited by gravity wave drag in the lower mesosphere partially contributed to vortex splitting at 10 hPa through downward propagation. With regard to the mechanisms driving the eastward-traveling PW2, Iida et al. (2014) proposed wind shear instability as a localized source, whereas Rhodes et al. (2021) attributed it to the over-reflection of upward-propagating tropospheric PW2. Yoo et al. (2023, hereafter YCK23) demonstrated that unstable PW2, spontaneously generated within the stratosphere, played a significant role in vortex splitting during the SSW event in 2021 (hereafter, SSW21).

70

79

- 71 This study examines whether in situ-excited PWs contributed to the polar vortex split during the first and only SSW event in
- 72 the SH, as observed in several NH SSWs. Specifically, this research identifies the spontaneous excitation of PWs in the mid-
- 73 to-upper stratosphere and their subsequent downward propagation toward 10 hPa—a feature overlooked in previous studies
- 74 on SSW02, which focused on altitudes at or below 10 hPa. Thus, building on the approach adopted in YCK23, this study
- 75 seeks to determine the in situ source of these waves and clarify the underlying preconditioning mechanism. In this context,
- 76 we draw comparison with SSW21, the focus of YCK23, to examine similarities and differences in the governing dynamics.
- 77 As we are aware, this study is the first to investigate the role of locally generated PWs in the development of SSW02,
- 78 offering deeper insight into the processes driving its occurrence.

2 Data and analysis methods

80 2.1 Modern-Era Retrospective analysis for Research and Applications, version 2 (MERRA-2) data

- 81 This study utilizes MERRA-2 reanalysis data on 42 standard pressure levels ranging from 1000 hPa to 0.1 hPa (Gelaro et al.,
- 82 2017). The data are provided at a horizontal resolution of $0.625^{\circ} \times 0.5^{\circ}$ (longitude × latitude) and a 3 h temporal resolution.
- 83 We use 44 years of data (1980–2023) for the analysis and all results presented are based on daily averages.

84 2.2 Analysis methods

85 2.2.1 Eliassen–Palm flux (EP-flux) and its divergence

- 86 The EP-flux and its divergence (EPFD), which represent wave activity flux and wave forcing, respectively, are calculated as
- 87 follows (Andrews et al., 1987):

88
$$\mathbf{F} = \left(F^{\phi}, F^{z}\right) = \rho_{0} a \cos \phi \left(-\overline{u'v'} + \overline{u}_{z} \frac{\overline{v'\theta'}}{\overline{\theta}_{z}}, \left[f - \frac{1}{a \cos \phi} (\overline{u} \cos \phi)_{\phi}\right] \frac{\overline{v'\theta'}}{\overline{\theta}_{z}} - \overline{u'w'}\right), \tag{1}$$

89
$$\nabla \cdot \mathbf{F} = \frac{1}{a\cos\phi} \frac{\partial}{\partial\phi} \left(F^{\phi}\cos\phi \right) + \frac{\partial F^{z}}{\partial z}. \tag{2}$$

In the above equations, ϕ and z denote latitude and log-pressure height, respectively. ρ_0 represents the reference density, a denotes Earth's mean radius, and f denotes the Coriolis parameter. The parameters u, v, and w correspond to the zonal, meridional, and vertical wind components, respectively, while θ denotes potential temperature. The overbar $\overline{()}$ and prime (') denote the zonal mean and deviations from the zonal mean, respectively. The EP-flux vector, denoted as \mathbf{F} , consists of meridional (F^{ϕ}) and vertical (F^{z}) components. EPFD is defined as $(1/\rho_0 a \cos \phi)\nabla \cdot \mathbf{F}$.

2.2.2 Barotropic (BT)-baroclinic (BC) instability

96 The evaluation of BT-BC instability is based on the meridional gradient of the quasi-geostrophic potential vorticity (QGPV)

97 in spherical coordinates (Andrews et al., 1987):

95

99 100

101

102103

104

105

106

110

111112

113

98
$$\frac{\partial \bar{q}}{a \partial \phi} = \frac{2\Omega \cos \phi}{a} - \frac{1}{a^2} \frac{\partial}{\partial \phi} \left[\frac{1}{\cos \phi} \frac{\partial (\bar{u} \cos \phi)}{\partial \phi} \right] - \frac{1}{\rho_0} \frac{\partial}{\partial z} \left(\rho_0 \frac{f^2}{N^2} \frac{\partial \bar{u}}{\partial z} \right), \tag{3}$$

where \bar{q} is the zonal-mean QGPV. Ω and N denote the rotation rate of Earth and the Brunt-Väisälä frequency. The first term corresponds to the meridional gradient of f. In Sect. 3 and Text S1, we define the second term on the right-hand side as the barotropic term, while the third term is designated as the baroclinic term. The necessary condition for BT-BC instability is met when the typically positive meridional gradient of the zonal-mean QGPV (hereinafter \bar{q}_y , where $y = a\phi$) associated with wintertime circulation, turns negative (Salby, 1996). This corresponds to one of the Charney-Stern-Pedlosky instability criteria, while under typical midlatitude conditions, the instability criterion is generally satisfied through both positive \bar{q}_y and positive $\frac{\partial \bar{u}}{\partial x}$ at the lower boundary (see Vallis, 2017 for details).

2.2.3 Linearized disturbance QGPV equation

107 In log-pressure coordinates, the linearized disturbance OGPV equation is expressed as follows (Matsuno, 1970):

$$\left(\frac{\partial}{\partial t} + \bar{u}\frac{\partial}{a\cos\phi\partial\lambda}\right)q' + v'\frac{\partial\bar{q}}{a\partial\phi} = \frac{1}{a\cos\phi}\left[\frac{\partial Y'}{\partial\lambda} - \frac{\partial(X'\cos\phi)}{\partial\phi}\right] + \frac{f}{\rho_0}\frac{\partial}{\partial z}\left[\rho_0\frac{Q'}{e^{\frac{\kappa}{H^Z}}\left(\frac{\partial\bar{T}_0}{\partial z} + \frac{\kappa\bar{T}_0}{H}\right)}\right],\tag{4}$$

$$q' \equiv \frac{1}{fa^2} \left[\frac{1}{\cos^2 \phi} \frac{\partial^2 \Phi'}{\partial \lambda^2} + \frac{f^2}{\cos \phi} \frac{\partial}{\partial \phi} \left(\frac{\cos \phi}{f^2} \frac{\partial \Phi'}{\partial \phi} \right) + \frac{f^2 a^2}{\rho_0} \frac{\partial}{\partial z} \left(\frac{\rho_0}{N^2} \frac{\partial \Phi'}{\partial z} \right) \right]. \tag{5}$$

In the above equations, λ denotes longitude, and q' represents the QGPV perturbation. The perturbations of the zonal and meridional components of gravity wave drag (GWD) from their zonal mean are represented by X' and Y', respectively. Q' denotes the perturbation diabatic heating rate and Φ' represents GHP. On the right-hand side of Eq. (4), the first bracketed term represents the nonconservative forcing term of the QGPV perturbation associated with GWD (Song et al., 2020). We

investigate whether the nonconservative GWD forcing, defined as Z' below, contributed to the vortex split using the zonal and meridional components of the parameterized GWD data (McFarlane, 1987; Molod et al., 2015).

116
$$Z' = \frac{1}{a\cos\phi} \left[\frac{\partial Y'}{\partial\lambda} - \frac{\partial (X'\cos\phi)}{\partial\phi} \right]$$
 (6)

117 2.2.4 Squared refractive index

118 To investigate PW propagation, we use the squared refractive index, defined as (Andrews et al., 1987)

119
$$n^2 = \left[\frac{\overline{q}_{\phi}}{a(\overline{u} - C_x)} - \left(\frac{k}{a \cos \phi} \right)^2 - \left(\frac{f}{2NH} \right)^2 \right] a^2, \tag{7}$$

- 120 where k denotes the nondimensional ZWN, and C_x represents the zonal phase speed of the wave. PWs can propagate in
- 121 regions where n^2 is positive, whereas their propagation is impeded in regions where n^2 is small or negative (Karoly and
- 122 Hoskins, 1982).

123 3 Results

124

132

133

3.1 Variations in wind and temperature during SSW02

- 125 Figure 1 presents the temporal evolution of the zonal-mean zonal wind at 60°S and the polar cap temperature over 60–90°S
- 126 during SSW02 development. The reversal of zonal-mean westerlies to easterlies began in the lower mesosphere on 22
- 127 September and progressed down to 10 hPa within three days, marking the onset of major SSW02 (Charlton and Polyani,
- 128 2007). Over the following week (18–25 September), the PNJ weakened dramatically by more than 57 m/s, accompanied by a
- 129 sudden temperature increase of approximately 20 K at 10 hPa. The deceleration and eventual reversal of the westerlies fall
- 130 below the 0.5th percentile of the 44-years of zonal-mean zonal wind record, while the associated temperature rise exceeds
- the 99.5th percentile of the corresponding temperature data.

3.2 Dynamical features of the vortex split and associated PW activities

- 134 Figure 2a offers an overview of the polar vortex split during the onset of SSW02 by illustrating the geopotential height
- perturbation (GHP) and horizontal wind fields at 10 hPa. By 21 September, the vortex had weakened and shifted away from
- the pole, and from 23 September, it elongated and ultimately split into two distinct vortices. The associated PW activities are
- analyzed by examining the evolution of ZWN1 and ZWN2 PW amplitudes at 60°S (Fig. 2b). In the days leading up to the
- onset, ZWN1 PW (PW1) had a greater amplitude than PW2 until 23 September, after which it rapidly weakened. Conversely,
- 139 PW2 intensified and surpassed the amplitude of PW1 at 10 hPa for two days following the onset. This anticorrelation
- between PW1 and PW2 is a common feature of split-type SSW events, including SSW21. However, PW activity during

SSW02 differed markedly from that during SSW21. Specifically, during SSW02, PW2 was enhanced from the upper troposphere with its amplitude exceeding the 97.5th percentile of the 44-year climatology. In contrast, during SSW21, PW2 strengthened within the mid-stratosphere (Fig. 1b of YCK23). This suggests that PW2, originating from the troposphere, played a crucial role in the vortex split during SSW02, aligning with previous findings (Krüger et al., 2005; Manney et al., 2005).

146

However, further insight is provided by the GHP of PW2 in the longitude–height cross sections depicted in Fig. 2c, which reveals an eastward tilt of the phase with increasing altitude above 3 hPa during the PW2 amplification period (21–25 September). This suggests downward-propagating PW2 from the mid-to-upper stratosphere, potentially contributing to PW2 intensification at 10 hPa.

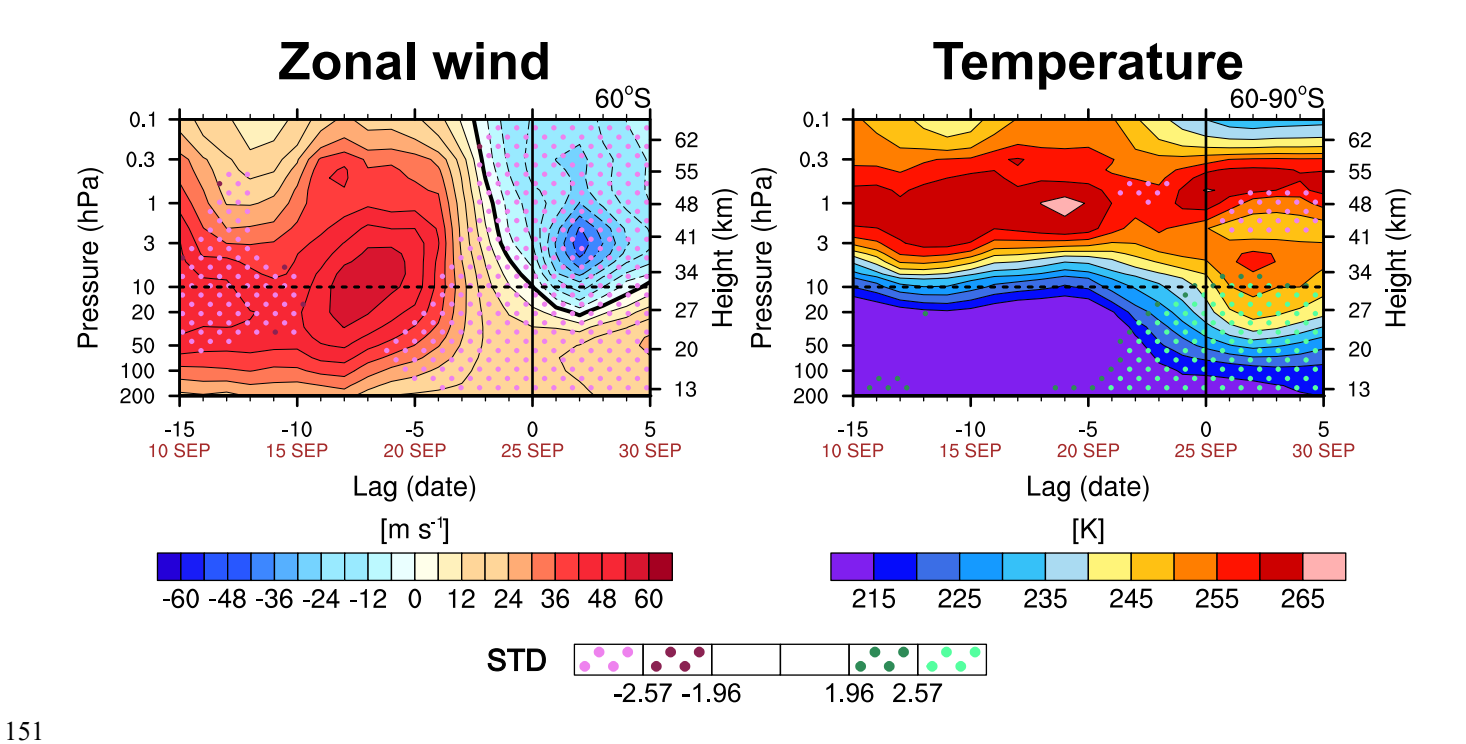


Figure 1: Time—height cross sections of the zonal-mean zonal wind at 60°S (left) and polar cap temperature averaged over 60–90°S (right). Dark and bright pink (green) dots indicate regions where the analyzed variable is algebraically smaller (larger) than its 44-year climatology by more than 1.96 and 2.57 standard deviations (STD), corresponding to values below the 2.5th and 0.5th percentiles (above the 97.5th and 99.5th percentiles), respectively.

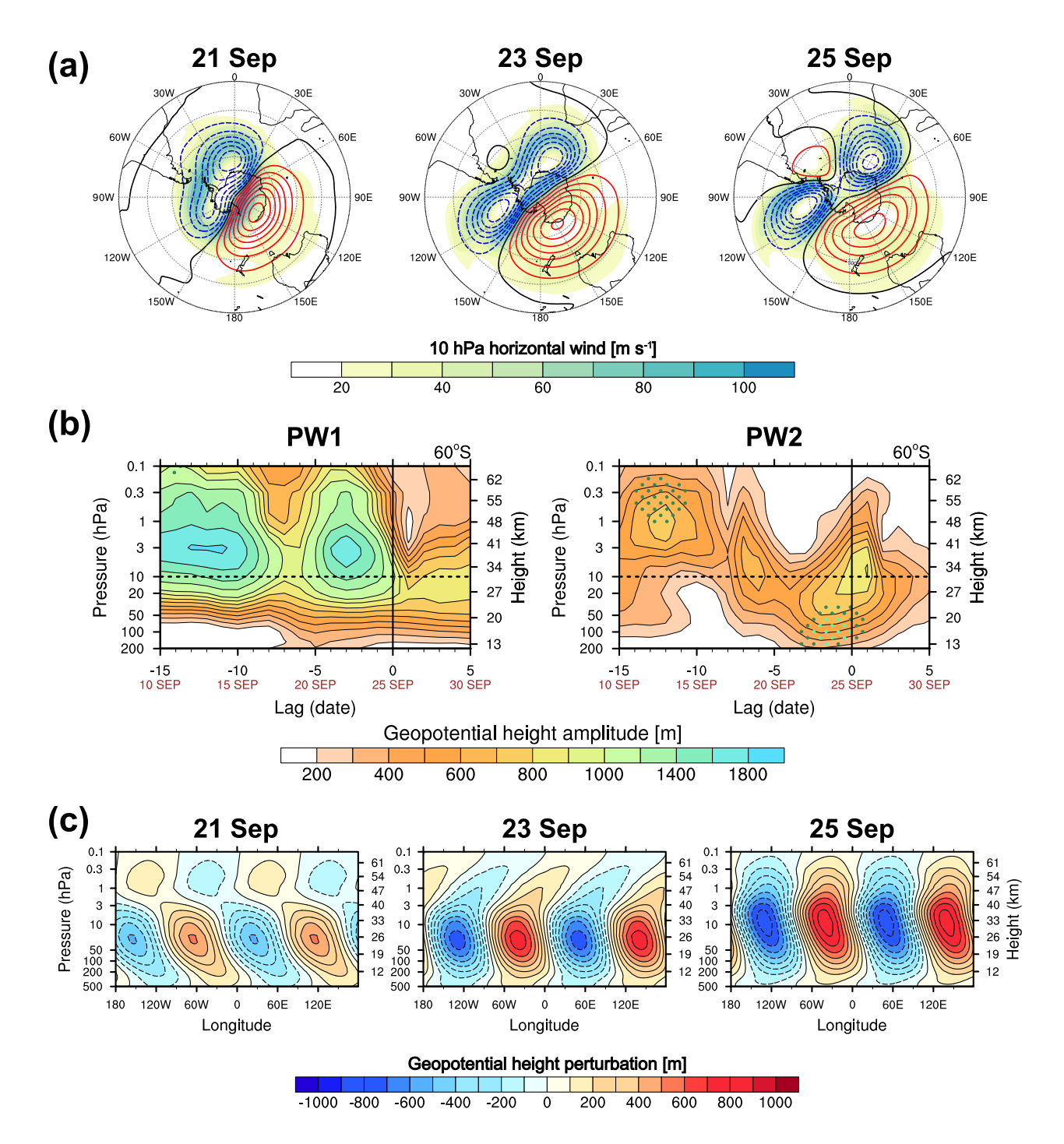


Figure 2: (a) Polar stereographic series showing horizontal wind speed (shading) and GHP from the zonal mean (contours) at 10 hPa on 21, 23, and 25 September 2002. Red (blue) contours denote positive (negative) values. (b) GHP amplitude of PWs with ZWN1 (PW1, left) and 2 (PW2, right) at 60°S. (c) Longitude–height cross sections of PW2 GHP on 21, 23, and 25 September 2002.

3.3 In situ source of the downward propagating PW2 in the mid-to-upper stratosphere

The downward-propagating signal of stratospheric PW2 is more evident in the EP-flux and EPFD, as depicted in Fig. 3a.

Beginning on 22 September, downward EP-fluxes emerged from the region of positive EPFD (70–50°S above 10 hPa),
which substantially overlapped with the easterlies descending from the polar mesosphere by 23 September. As the easterlies intensified and extended toward the equator, the positive EPFD also strengthened, reaching amplitudes above the 97.5th percentile. This indicates in situ PW2 excitation within the stratosphere and its dependence on the background atmospheric conditions. The downward- and equatorward-propagating stratospheric PW2 converged with upward-propagating tropospheric PW2 near 10 hPa and 60°S, leading to a significant negative EPFD falling below the 0.5th percentile.

The wave fluxes and forcings observed during SSW02 closely resembled those during SSW21 (Fig. 3a of YCK23), where BT-BC instability was the primary source of stratospheric in situ PW2 excitation. Accordingly, we examined the potential role of instability as a source by analyzing \bar{q}_y (Fig. 3b). Negative \bar{q}_y appeared within the easterly region and intensified as it expanded equatorward, mirroring the evolution of easterlies. Recognizing a similar pattern, YCK23 attributed the onset of instability to the strengthening easterlies, as follows: The positive meridional curvature of the easterlies (barotropic term) exceeded the beta effect, rendering the sum of two terms negative. Simultaneously, the negative shear and positive curvature of the easterlies caused the baroclinic term to turn negative. These factors collectively led to negative \bar{q}_y (see Figs. 3 and 4 in YCK23 for further details). The same diagnostic framework applied to the present case shows consistent results (see Fig. S1 and Text S1). The region of instability partially overlapped with the area of PW2 generation. All these features, consistent with YCK23, indicate that strong shear instabilities driven by strengthening easterlies promoted unstable PW2 growth within the stratosphere during SSW02.

Zonally asymmetric GWD could also generate PWs in situ in the upper stratosphere and lower mesosphere through the nonconservative forcing (Z') of the linearized disturbance QGPV (Eq. 4-6). Song et al. (2020) reported that the significant PW2 amplification at 10 hPa, which led to the splitting of the polar vortex during the 2009 SSW, was partially attributed to the downward-propagating PW2 generated in situ by ZWN2-patterned GWD in the lower mesosphere. Yoo et al. (2024) revisited this excitation mechanism using an idealized general circulation model and demonstrated that PWs induced by Z' led to substantial fluctuations and forcings as they propagated. To examine whether stratospheric PW2 is associated with GWD via Z', we analyzed the magnitude of ZWN2 Z' along with the divergence of PW2 EP-fluxes (Fig. 3c). Notably, ZWN2 Z' showed a large amplitude primarily in the upper stratosphere and lower mesosphere (0.3–0.1 hPa), where PW2 generation by GWD occurred during the 2009 SSW, as identified by Song et al. (2020). However, these areas did not coincide with the key region of PW2 excitation (5-1 hPa) during SSW02. Even within the lower mesosphere, Z' in the 60-70°S region, where positive EPFD appeared, was weaker than that in other latitudinal regions. Therefore, as in SSW21, instability was identified as the most likely source of PW2 in this case.

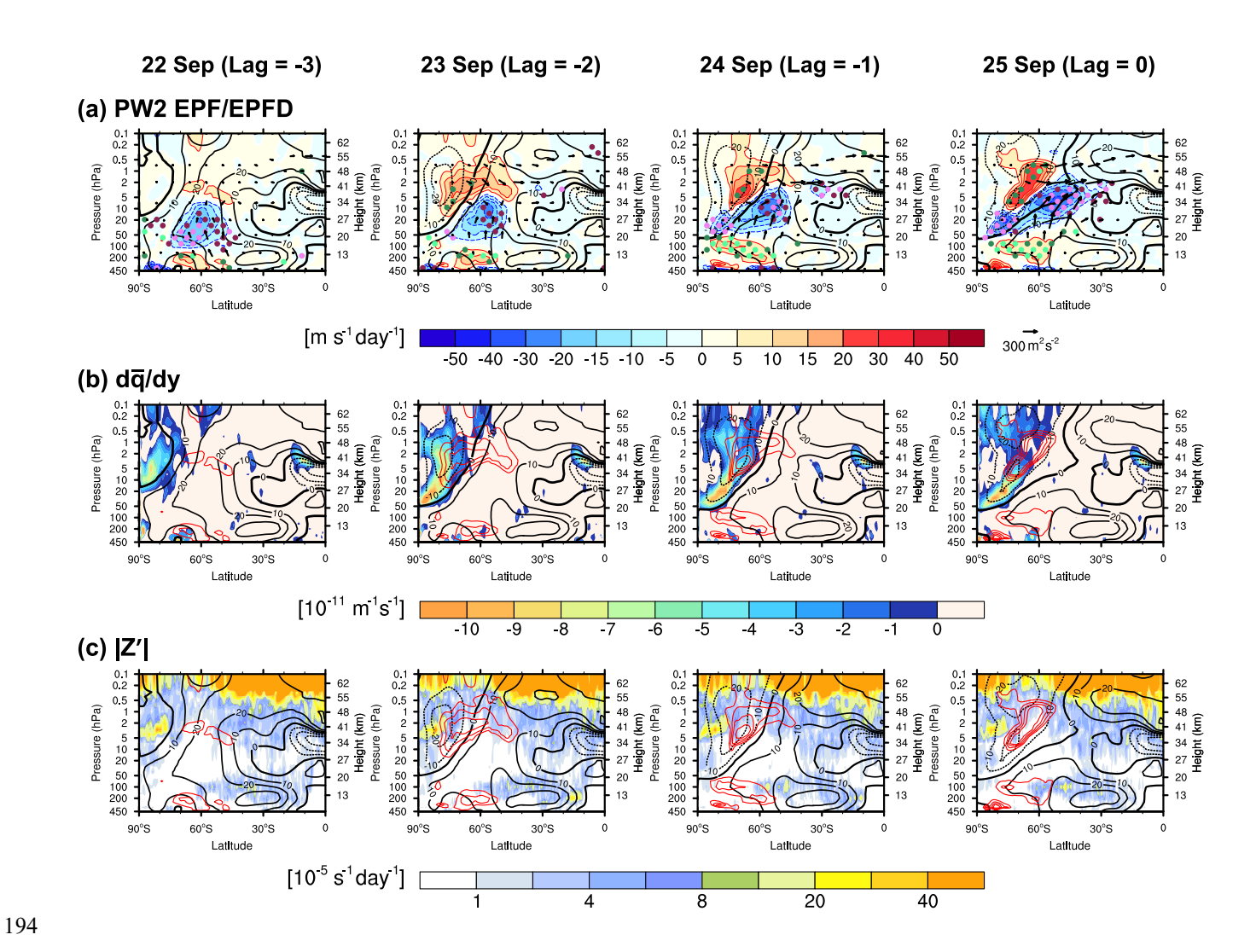


Figure 3: Latitude-height cross sections of (a) the EP-flux (vectors) overlaid on its divergence (EPFD, shading) for PW2, (b) negative meridional gradient of the zonally averaged quasi-geostrophic potential vorticity (\bar{q}_y , colors) overlaid with the positive EPFD of PW2 (red contours), and (c) magnitude of the ZWN2 component of nonconservative GWD forcing on the quasi-geostrophic potential vorticity perturbation (Z', shading) overlaid with the positive EPFD of PW2 (red contours) from 22 to 25 September 2002. Black contours represent zonal-mean zonal wind, with solid, dashed, and thick solid lines indicating positive, negative, and zero wind, respectively. For visualization, EP-flux vectors in (a) are scaled using Eq. (18) and Table 2 of Jucker (2020), and additionally divided by the square of Earth's radius.

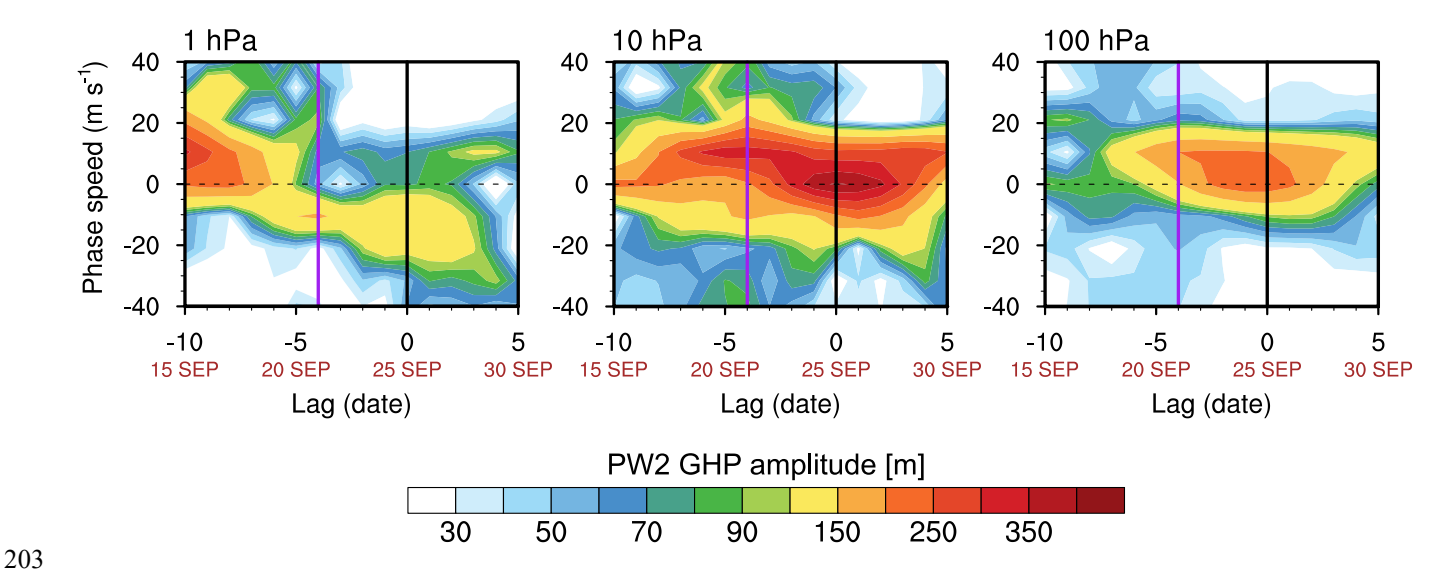


Figure 4: Time–zonal phase speed cross sections of PW2 GHP amplitude averaged over 60° S at 1, 10, and 100 hPa, derived from 2D (zonal, time) Fourier decomposition of GHP using an 11-day sliding window (Song et al., 2020). To reduce edge effects, the first and last 3 days of the window are tapered using sine and cosine functions, respectively. Zonal phase speed (C_x) is calculated as ω/k , where ω is frequency and k is zonal wavenumber. The purple and black vertical lines indicate the start date of PW2 amplification and the onset date, respectively.

209 An inspection of the zonal phase speed of in situ-excited PW2 supports this hypothesis. Instability destabilizes PWs whose 210 zonal phase speed matches the zonal wind speed in the instability region (Dickinson, 1973). Figure 4 illustrates the time-211 zonal phase speed cross sections of the PW2 GHP amplitude at 1, 10, and 100 hPa. In line with Dickinson's argument, the 1 212 hPa PW2 predominantly exhibited westward phase speeds during the generation period of mid-to-upper stratospheric PW2 (22-25 September). Furthermore, its dominant phase speed range of -5 to -25 m s⁻¹ aligns well with the easterlies in the 213 instability region (-25-0 m s⁻¹; Fig. 3b). However, the possibility that these waves originate from below cannot be entirely 214 215 ruled out. Although westward-propagating PW2 (WPW2) exhibit smaller amplitude at 100 hPa (accounting for ~29% of 216 total GHP amplitude), they can propagate up to 1 hPa under the prevailing wind structure, featuring a transition from westerlies to easterlies with height (Fig. 3a), in accordance with the Charney and Drazin (1961) criterion $[0 < u - C_r < v]$ 217 $u_c = \beta/(k^2 + l^2 + \frac{f_0}{4H^2N^2})$, where l and f_0 represent the meridional wavenumber and Coriolis parameter at latitude ϕ_0 , 218 219 respectively]. It contrasts with the dominant eastward-propagating PW2 at 100 hPa, whose upward propagation is prevented 220 by the vertical wind reversal. Nonetheless, the 1 hPa WPW2 is unlikely to be a simple continuation of those from below, 221 given the distinct positive EPFD indicative of local wave amplification (Fig. 3a). All accumulated evidence suggests that 222 stratospheric WPW2 arose spontaneously from their critical levels within the instability region.

These in situ-excited WPW2 influenced the enhancement of PW2 at 10 hPa through downward propagation. This is evidenced by the phase speed range of WPW2 across different altitudes. While the phase speed of WPW2 at 100 hPa was largely below 10 m s⁻¹, it increased to above 30 m s⁻¹ at 10 hPa, aligning with the phase speed range observed at 1 hPa.

227 These findings confirm that in situ-excited WPW2 at 1 hPa contributed to amplifying PW2 at 10 hPa. Notably, this

228 contribution persisted even after the onset date.

223

229

230

231232

233

234

235

236237

238

239

3.4 Vortex preconditioning: poleward shift of the polar vortex

Consistent with SSW21, the evolution of easterlies within the polar stratosphere drove the vortex toward BT–BC instability during SSW02. This raises the question of whether SSW02 was also preceded by double-westerly jets and their critical-level interaction with tropospheric PWs, which led to zonal wind reversal and associated instability during SSW21. To address this, we analyzed the evolution of zonal-mean zonal winds from 20 September to the onset date (Lag = –5 to 0), as shown in Fig. 5. A double-westerly jet–like configuration evident on 21 September, with one core in the polar stratosphere and another in the subtropical mesosphere, had been present since early September (not shown). However, the equatorial stratospheric easterlies that propagated toward the polar stratopause along the path between the two cores and eventually dominated the polar stratosphere—a phenomenon observed in SSW21 (see Fig. 7 of YCK23)—were not identified in SSW02. Instead, easterlies emerged from the polar mesosphere on 21 September (Lag = –3) and rapidly descended into the lower stratosphere.

Zonal-mean zonal wind

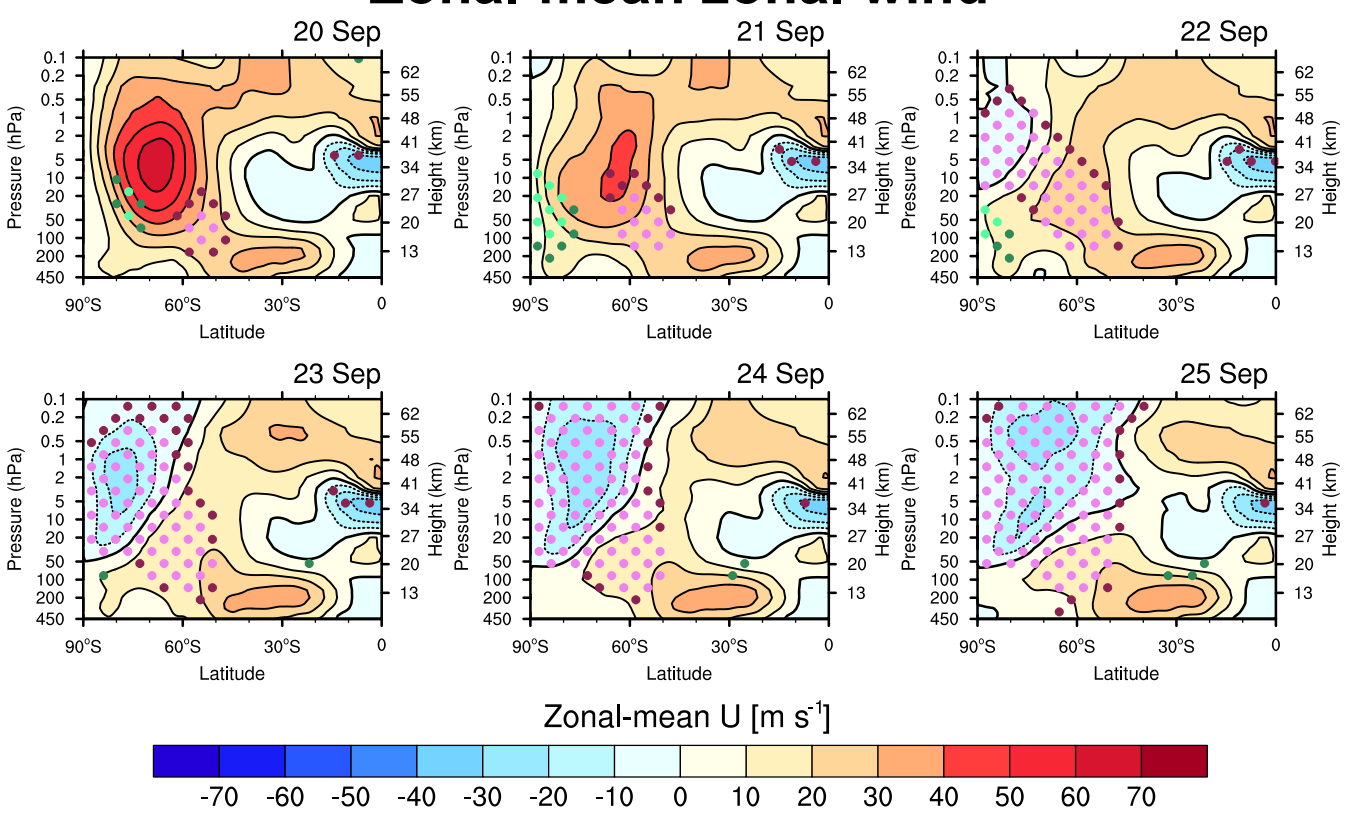


Figure 5: Latitude—height cross sections of zonal-mean zonal wind in the SH from 20 to 25 September 2002.

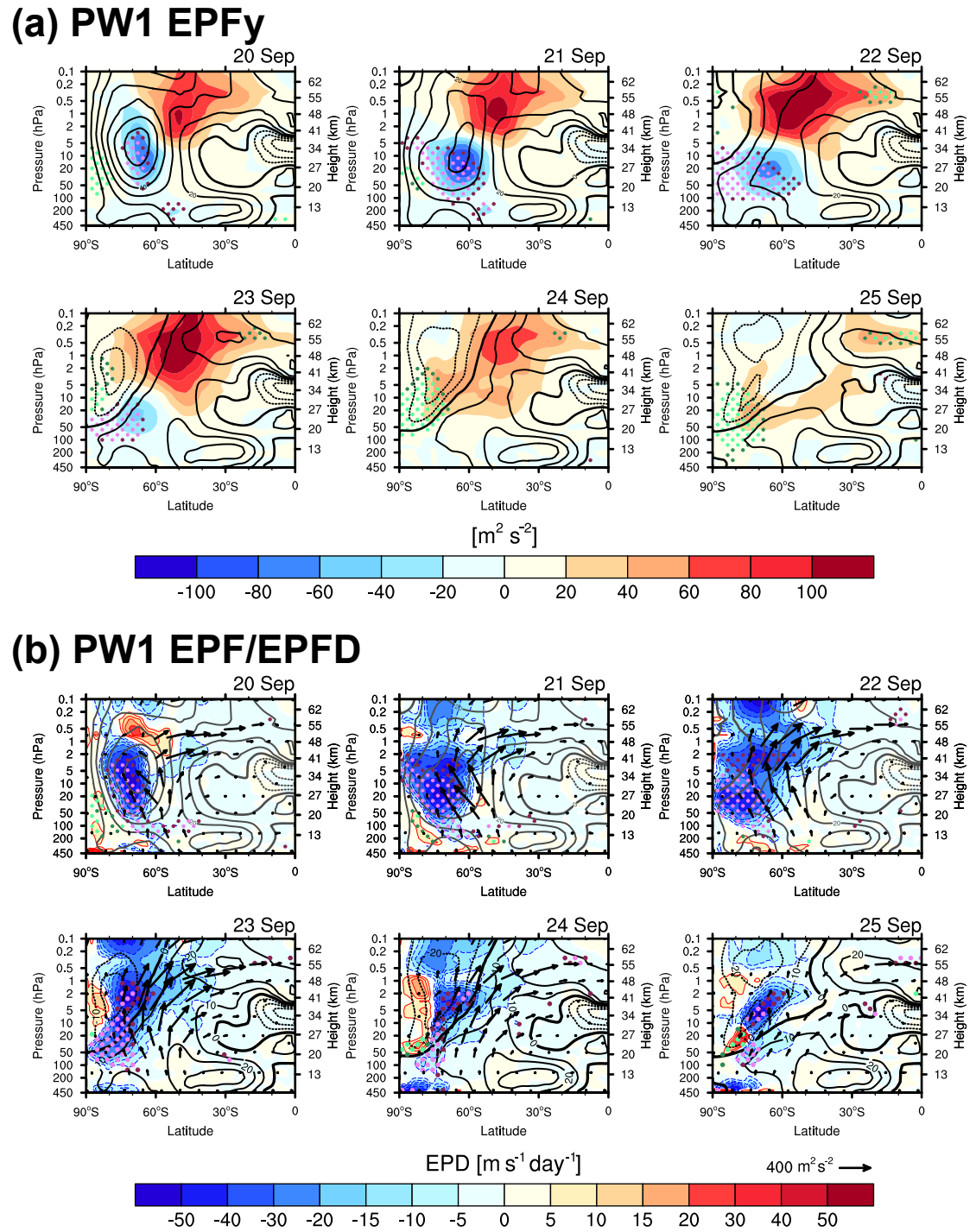


Figure 6: Latitude—height cross sections of (a) the meridional component of EP-flux (EPFy, shading) and (b) EP-flux (vectors) overlaid on EPFD (shading) for PW1 from 20 to 25 September 2002. EP-flux vectors are scaled following the same method as in Fig. 3. Black contours indicate zonal-mean zonal wind, with the contour specifications identical to those in Fig. 3.

248 An abrupt development of easterlies was preceded by the abnormal increase (decrease) in the zonal-mean zonal wind on the 249 poleward (equatorial) side of the jet streak on 20–21 September. This is consistent with the poleward shift of the PNJ relative 250 to climatology, as documented by Newman and Nash (2005), although they noted that this shift had begun as early as April. 251 Throughout the winter period, this shift guided irregular bursts of tropospheric waves toward higher latitudes, enhancing 252 westward momentum transfer into the polar region. While Fig. 5 focuses on the period of rapid wind transition, a feature supporting this argument is evident in the meridional component of EP-flux (F^{ϕ}) and EPFD of PWs during this period (Fig. 253 6). The focus here is on PW1, which predominantly induced negative PW forcing, facilitating the transition from westerlies 254 to easterlies (Fig. S2). From 20 to 21 September, F^{ϕ} exhibited significant negative values along the vortex center, falling 255 below the 0.5th percentile. This confirms an unusual progression of PW1 toward higher latitudes, guided by the poleward-256 displaced vortex. Following the rapid weakening and transition of the PNJ into easterlies, a substantial negative F^{ϕ} value 257 258 gradually extended to lower altitudes by 23 September. These waves deposited significant negative EPFD, ranked below the 0.5th percentile, with a maximum of approximately 50 m s⁻¹ day⁻¹ near the jet maximum on 21 September (Fig. 6b). 259 260 Exceptionally strong westward momentum from PW1 facilitated the transition of westerlies to easterlies from the polar 261 mesosphere. Positive feedback via critical-level interaction between the zero-wind line and subsequent tropospheric PW1 262 further enhanced the downward expansion of polar easterlies with increasing intensity.

263

The next key question concerns the mechanisms driving the unusual poleward displacement of the vortex. Newman and Nash (2005) and Gray et al. (2005) identified anomalous easterlies in the equatorial upper stratosphere (1–10 hPa) as a potential factor contributing to the poleward vortex shift. Gray et al. (2005) proposed that these upper stratospheric easterlies over the equator generated strong horizontal wind shear and steep PV gradients in the SH subtropics during early winter, effectively confining equatorward-propagating PWs to the polar upper stratosphere. In this context, they suggested that the tropical stratopause's SAO as a favorable precursor to SSW.

3.5 Destabilization of ZWN2 waves

During SSW21, irreversible PV mixing driven by an exceptionally strong PW1 breaking led to the formation of a secondary cyclone and BT–BC instability, suggesting the destabilization of WPW2 in the mid-stratosphere (YCK23). This aligns with McIntyre's (1982) proposal that large amplitude wave breaking disrupts the basic equator-to-pole PV gradient, creating an atmosphere characterized by scattered pieces of high and low PV. Under such conditions, energy cascades from low to high wavenumbers across the PV and height fields to preserve enstrophy and energy. The abnormal PW1 breaking (Fig. 6b) and the temporally out-of-phase relationship, wherein PW1 weakened as PW2 strengthened (Fig. 2b), suggest that a similar phenomenon may have occurred during SSW02.

277278

270

271272

273

274

275

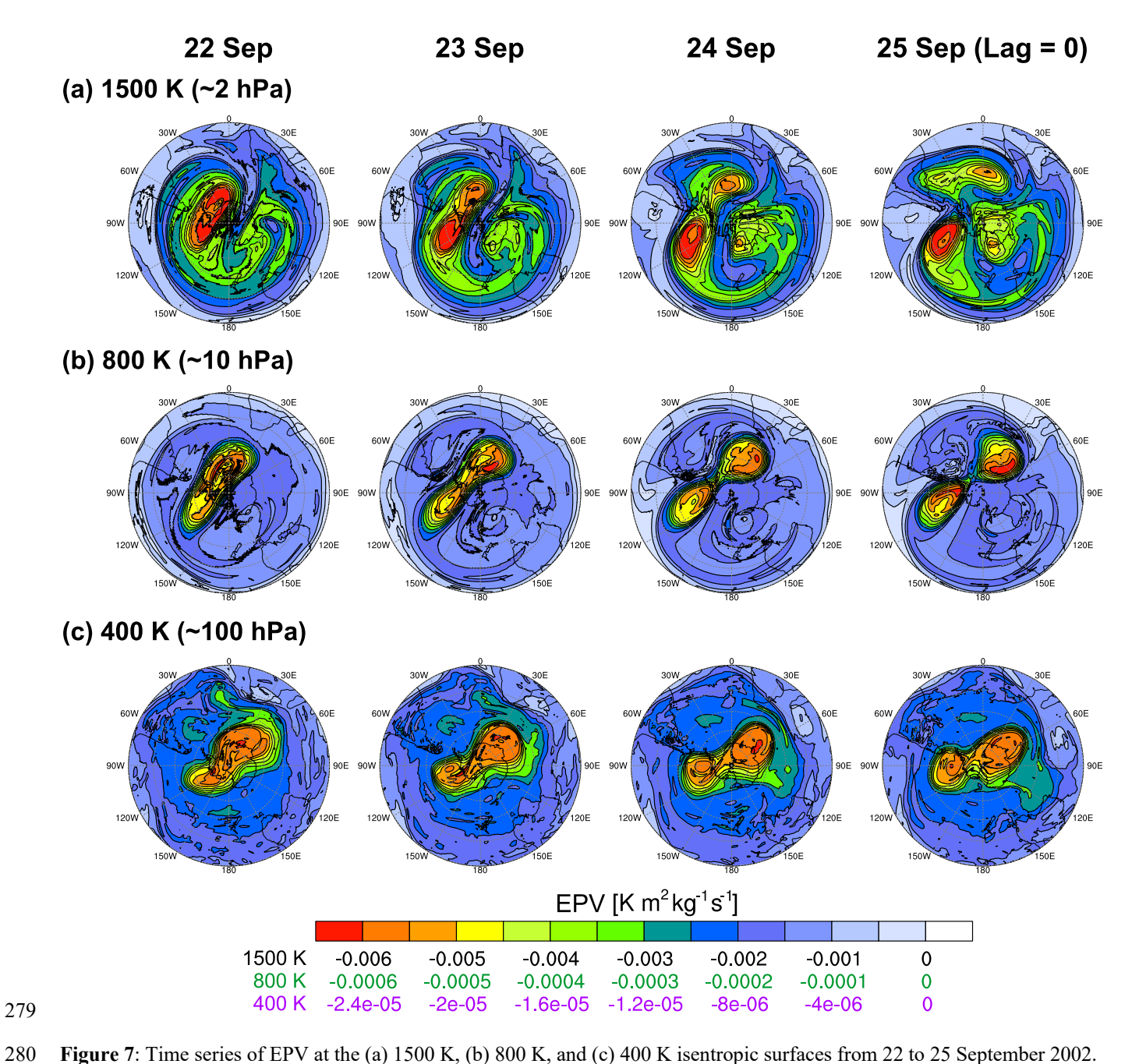


Figure 7: Time series of EPV at the (a) 1500 K, (b) 800 K, and (c) 400 K isentropic surfaces from 22 to 25 September 2002.

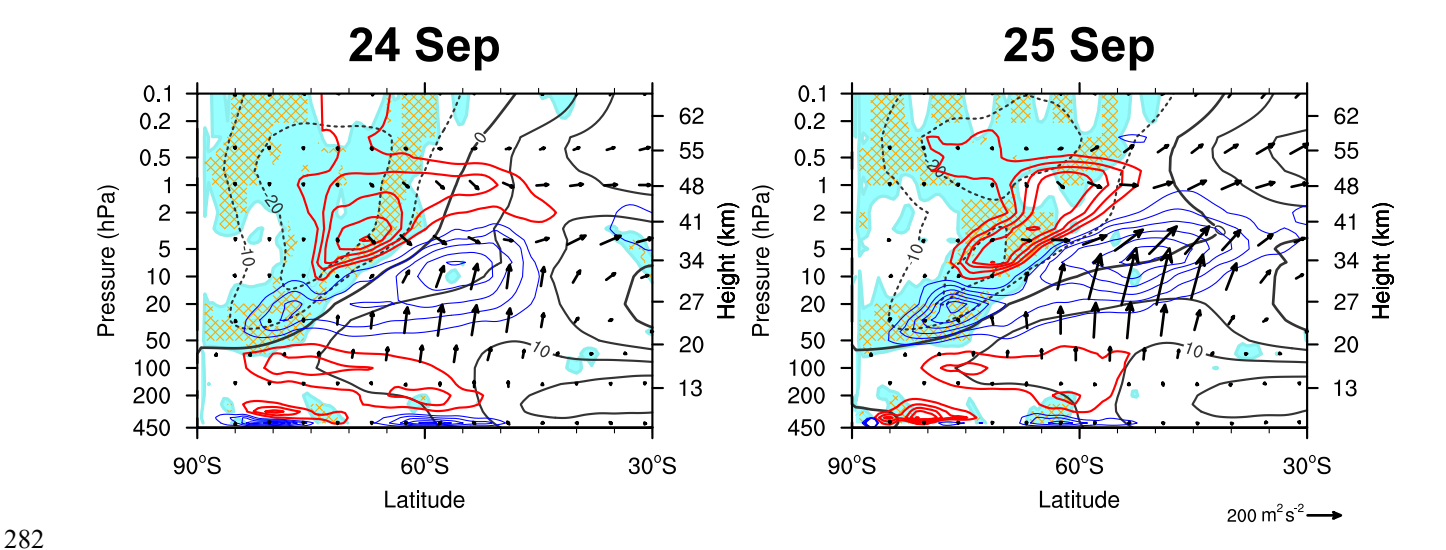


Figure 8: Latitude—height cross sections of the negative meridional gradient of zonally averaged quasi-geostrophic potential vorticity (\bar{q}_y , mint shading) and negative squared refractive index (n^2 , orange hatching) within the instability area overlaid with PW2 EP-flux (vectors) and EPFD (contours, where red and blue indicate positive and negative values, respectively) on 24–25 September 2002. Black contours represent zonal-mean zonal wind, with contour specifications matching those in Fig. 3. The contour intervals for the red and blue lines are identical to those shown in the color bar of Fig. 3a. EP-flux vectors are scaled following the same method as in Fig. 3.

The evolution of Ertel's PV (EPV) on the 1500 K isentropic surface (approximately 2 hPa) in Fig. 7a closely resembles that observed during SSW21 (Fig. 8 of YCK23). On 22 September, significant PW1 breaking and the resulting irreversible mixing strongly deformed the vortex, ultimately forming an additional cyclone in its trailing region (90°E–180°). Simultaneously, low magnitude PV extended deeply into higher latitudes, crossing the pole between two high magnitude PV cores. This indicates a localized reversal of the meridional PV gradient, destabilizing the flow. These features suggest that PW1 breaking triggered smaller-scale wave generation through energy cascading and initiated BT–BC instability, which could further amplify these smaller-scale waves. This process likely contributed to PW2 enhancement in the mid-to-upper stratosphere.

Unlike SSW21, SSW02 involved the separation of the primary cyclone, which began on 23 September. Wavenumber decomposition revealed that this separation accounted for the substantial amplification of PW2 from 24 September (not shown). The formation of the secondary cyclone and its subsequent eastward migration at the 1500 K isentropic surface can be traced back through the 800 K isentropic surface (approximately 10 hPa, Fig. 7b) to structures originating in the lower stratosphere near 400 K (approximately 100 hPa, Fig. 7c). The GPH at 100, 10, and 2 hPa in the supplementary material (Fig. S3) supports this interpretation: At 100 hPa, a clear ZWN2 pattern appears from 22 September, while at 10 hPa, the primary cyclone evolves into a peanut-like structure on 23 September, followed by a vortex split on 24 September. A similar sequence occurs at 2 hPa with a one-day delay, indicating the vertical extension of PW2 features. Based on earlier evidence supporting in situ WPW2 generation in the mid-to-upper stratosphere via BT–BC instability, this upward-propagating signal suggests that unstable WPW2 excitation is associated with the incident PW2 from below. This seemingly counterintuitive interpretation can be understood in the context of the over-reflection of waves from below.

The concept of over-reflection relates incident PWs to the in situ PW excitation through BT-BC instability (Rhodes et al., 2021). As previously mentioned, a critical layer embedded within an unstable region (with $\bar{q}_{\nu} < 0$) can be a source for unstable PW growth (Dickinson, 1973). If incident PWs can tunnel from the turning level (where waves first become evanescent) to the critical level (where $\bar{u} = C_x$) through the evanescent region (where $n^2 < 0$ owing to $\bar{q}_v < 0$ and $\bar{u} - C_x > 0$ 0), these waves can grow by extracting energy from the mean flow. From this perspective, the growth of unstable PWs is initiated by PWs tunneling beyond the turning level and amplifying at the critical level (e.g., Harnik and Heifetz, 2007). Over-reflection occurs when an incident PW is reflected from the turning level, gaining more energy than it originally had (Rhodes et al., 2021) and the divergence of EP-flux represents this energy growth. Figure 1 and the related discussion in the paper by Rhodes et al. (2023) provide further details.

The possibility of over-reflection is explored in Fig. 8, which presents latitude-height sections of PW2 EP-fluxes and EPFD along with the evanescent region (negative n^2 , orange hatching) within the destabilized area (negative \bar{q}_{ν} , cyan shading).

This figure focuses on 24–25 September, when the primary cyclone became fully detached. Here, n^2 is calculated by setting ZWN k=2 with a zonal phase speed C_x of -20 m s⁻¹. As the magnitude of negative C_x increases, the evanescent region expands toward the easterly core due to the increasing area where $\bar{u} - C_r > 0$, leading to $n^2 < 0$. Thus, the negative n^2 with the selected C_x (-20 m s⁻¹) roughly encompasses the evanescent region derived from the major C_x range of WPW2 propagating upward from 100 hPa (-20-0 m s⁻¹, Fig.4), which are subject to over-reflection in the destabilized polar stratosphere dominated by easterlies. Some of the upward-propagating PW2, whose westward components increase with height (as discussed in Section 3), encountered the lower boundary of the WPW2 evanescent region, where the incident WPW2 were able to tunnel through. From the critical levels above the evanescent region, downward and equatorward PW2 fluxes emerged, increasing in magnitude with distance, thereby creating a positive EPFD. All these features suggest that the growth of stratospheric WPW2 was associated with the westward component of incident PW2 tunneling to their critical levels through the evanescent region and subsequent amplification at those levels. As such, the downward propagation of PW2, opposite to the upward-propagating incident PW2, is interpreted as over-reflection, with the positive EPFD indicating that these waves had greater energy than the incident ones. While the positive EPFD region extends farther equatorward, the area of potential PW generation via instability remained largely confined to higher latitudes on 24 September (Fig. 8), reflecting a similar pattern observed on 23 September (Fig. 3b). This is likely because \bar{q}_{ν} , calculated using zonal-mean variables, does not fully capture the longitudinally varying instability extending into lower latitudes. Such instability, inferred from the negative meridional gradient of EPV on 1500 K isentropic surface (Fig. S4), appear over broad longitudinal bands, although it is not zonally continuous. These spatially extensive unstable regions suggest a potential for amplifying even planetary-scale waves, though idealized modeling studies are needed to substantiate this inference.

323

324

325

326327

328

329

330

331

332

333

334335

336

337338

339

340

341

342343

344

345

346

347

348

349

350

351

352

353

The nonlinear wave—wave interaction process—the development of easterlies resulting from PW1 dissipation (Fig. 6b), the associated onset of instability (Fig. 3b), and the emergence of an additional cyclone in the tailing region of the parent cyclone (Fig. 7a)—was active by 22 September and persisted through 25 September. In contrast, as shown in Fig. 3a–3b, over-reflection was unlikely until 23 September, as upward-propagating PW2 did not reach their critical levels within the unstable region, which confined to high latitudes (poleward of 60°S). From 24 September onward, however, the easterlies extended downward and equatorward, coinciding with intensified upward-propagating PW2—as indicated by the enhanced EP-flux—such that the waves reached the turning level and over-reflection occurred (Fig. 8). This suggests that wave—wave interactions appear to dominate the early phase of wave generation, whereas over-reflection likely contributed to the later phase. Determining which mechanism played the dominant role would require a quantitative comparison, which remains beyond the scope of this study.

4 Summary and Discussion

Since the initiation of routine upper-atmosphere observations, only one SSW has been recorded in the SH, occurring on 25 September 2002. This SSW event was marked by the splitting of the polar vortex, a phenomenon rarely observed even in the NH. Early studies in the 2000s primarily examined the role of tropospheric PWs and vortex preconditioning, which direct these waves toward the polar stratosphere, in triggering SSW02. However, the influence of spontaneously generated waves within the stratosphere remains unexplored. Building on the recent findings of YCK23, which highlighted the critical role of instability-induced stratospheric waves in vortex splitting during the 2021 NH SSW, this study revisits SSW02, focusing on the potential contribution of in situ-excited PWs to the vortex split.

Consistent with previous studies, the substantial amplification of PW2 at 10 hPa, which led to the sudden split of the polar vortex, can be traced back to anomalous bursts of ZWN2 waves in the troposphere. However, this study also identifies the simultaneous descent of WPW2 from the mid-to-upper stratosphere to 10 hPa, suggesting their contribution to the vortex split. These WPW2s were generated in situ within the polar stratosphere, which was driven toward BT–BC instability as the zonal wind reversal progressed downward from the lower mesosphere including the WPW2 critical layer. These in situexcited WPW2 contributed to PW2 intensification at 10 hPa through downward propagation.

Instability amplified PW2 through two distinct mechanisms: nonlinear wave—wave interactions – similar to the process observed during SSW21 (YCK23) – and the over-reflection of upward-propagating PW2. Nonlinear wave—wave interaction involves PW1 breaking, which cascades energy into smaller-scale waves and simultaneously triggers instability, leading to the in-situ PW2 excitation. In the case of over-reflection, unstable PW2 growth occurred as upward-propagating PW2 tunnel through the evanescent layer and encounter a critical level embedded within the instability region. While these mechanisms operate through distinct pathways, nonlinear interaction induce stratospheric instability that favorable for over-reflection when incident PW2 is present—implying that the former may conditionally facilitate the latter. For SSW02, nonlinear interaction initiated the stratospheric PW2 amplification, setting up favorable conditions for over-reflection, which played a role nearer to the onset. Meanwhile, a double-jet configuration, previously proposed as a vortex preconditioning mechanism for inducing instability during SSW21 (YCK23), also preceded SSW02. However, unlike in SSW21, the critical-level interaction between the double-jet and tropospheric PW1 was absent in SSW02. Instead, an anomalous poleward shift of the polar vortex led to zonal wind reversal and vortex destabilization by confining PW1 to the polar stratosphere and enhancing westward momentum deposition in that region.

Common insights emerge from this study and YCK23, which examined SSW events across different hemispheres: Anomalous PW1 breaking leads to zonal wind transitions to easterlies, destabilizing the stratosphere during major SSW development. The subsequent growth of unstable PW2 contributes to polar vortex splitting. Among the 11 wave-2-type

major SSW events exhibiting vortex split characteristics in the NH over the 44-year period from 1980 to 2023 (classified by Ryoo and Chun 2005; Table S1), six cases present the simultaneous occurrence of PW1 dissipation, BT–BC instability, and PW2 generation within the stratosphere (Fig. S5–S10). Although this assessment is based on a preliminary visual inspection disregarding time lag among these phenomena, it suggests that in situ PW2 generation via instability could have contributed to approximately half of vortex-splitting SSW events. This highlights the role of explosive unstable PW growth within the stratosphere in vortex splitting, though this mechanism is not exclusive to split cases. Given the influence of in situ PW2 excitation via instability on vortex morphology—a key factor in shaping SSW characteristics and its downward influence—incorporating this mechanism into SSW research could provide a more comprehensive understanding of SSW dynamics.

Anomalous easterlies in the equatorial upper stratosphere are another shared feature between SSW02 and SSW21. The occurrence of both events during the westerly phase of the QBO in the lower stratosphere (50 hPa) – a condition that typically suppresses SSWs according to the Holton–Tan effect – supports the role of equatorial upper stratospheric winds in triggering SSWs. Notably, similar vortex shifts linked to equatorial upper stratospheric easterlies were also observed during the 2019 SH minor warming event. Additionally, Koushik et al. (2022) reported that equatorial easterlies in the upper stratosphere were present in approximately 70% of 29 NH SSW events from 1979 to 2021. They further highlighted a growing frequency of SSWs preceded by this wind structure since 2000, suggesting a shift in the system's dynamics. In this context, further research is warranted in two key areas: 1) the processes governing the development of anomalous equatorial upper stratospheric easterlies that trigger SSWs, particularly their connection to equatorial waves and lower stratospheric mean flows; 2) the reason underlying the increasing frequency of SSWs with these easterlies, linked to climate change. Considering the observational limitations in the equatorial upper stratosphere, a numerical modeling approach could help address these questions.

Two additional aspects deserve discussion—one concerning the data, the other the analytical approach. First, our analysis involves the upper stratosphere and lower mesosphere, where reanalysis reliability is limited due to the sparse assimilated observations; the only satellite observation used in MERRA-2 for that altitude—Aura Microwave Limb Sounder—was launched in 2004. This limitation is particularly important because the key arguments in our study involve the downward propagation of both zonal wind and PWs from higher altitudes. To provide support the validity of our results, we supplemented our analysis using two additional reanalysis datasets: the fifth generation of the European Centre for Medium-Range Weather Forecasts (ECMWF) Reanalysis re-run for 2000–2006 (ERA5.1, Simmons et al., 2020) and the Japanese Reanalysis for Three Quarters of a Century (JRA-3Q; Kosaka et al., 2024) (Text S2 and Fig. S11–13). While minor structural differences arise from the different resolutions and upper limit of the datasets—mainly in variables involving latitudinal or vertical derivatives such as EP-flux—all three reanalyses show broadly consistent zonal-mean flow and wave behavior. Despite limitations in representing the upper stratosphere and lower mesosphere, the consistency across reanalysis datasets suggests that our results reflect actual phenomena at those altitudes rather than dataset-specific artifacts.

425

426

427 428

429

430

431 432 Second, this study is primarily based on the classical wave—mean flow interaction framework. However, under highly distorted vortex conditions (as shown in Fig. 2 and 7), this approach may lead to oversimplification. This perspective was raised by O'Neill et al. (2017), who analyzed the same event. They showed that polar vortex splitting occurred as the vortex was already elongated and a sub-planetary scale closed cyclone (approximately zonal wavenumber 4) developed in the troposphere, barotropically aligned with one of the vortex tips. Under linear, steady-state atmospheric conditions, such a scale is unexpected to propagate upward into the stratosphere (Charney and Drazin 1961), indicating that vortex splitting involves processes beyond the upward propagation of PW2, including dynamical upscaling from the sub-planetary scale cyclogenesis to planetary scale responses. Therefore, interpreting this event based solely on PW components and non-local diagnostics, such as the EP-flux, may not fully capture the complex dynamics involved. While our EPV-based analysis (Fig. 7) focused on identifying non-linear processes and interpreting the cyclone's vertical structure through delocalized PW2 upward propagation, further investigation into non-linear PV advection and vortex–vortex interactions may provide

433434

435

Data availability

- 436 MERRA-2 data are provided by the Global Modeling and Assimilation Office (GMAO) at NASA Goddard Space Flight
- 437 Center and are available through the NASA GES DISC online archive (https://doi.org/10.5067/WWQSXQ8IVFW8; GMAO,
- 438 2015). ERA5.1 reanalysis data are available from the ECMWF via the Copernicus Climate Data Store
- 439 (https://apps.ecmwf.int/mars-catalogue/?type=an&class=ea&stream=oper&expver=51). JRA-3Q reanalysis data were
- obtained from the NCAR Research Data Archive (https://rda.ucar.edu/datasets/d640000/dataaccess/). The data supporting
- 441 this study's findings are available upon request from the corresponding authors.

additional insight into the dynamics of vortex splitting.

442 Author contributions

- 443 JHY and HYC conceived the study. JHY conducted the formal analysis and visualized the results. JHY drafted the
- 444 manuscript with contributions from HYC.

445 Competing interests

446 The authors declare no conflicts of interest.

447 Financial support

- 448 This research was supported by a National Research Foundation of Korea grant funded by the South Korean government
- 449 (2021R1A2C100710212).

450 Acknowledgement

- 451 We thank the three anonymous reviewers for their constructive and helpful comments. We also thank Dr. Han-Chang Ko for
- 452 his assistance with ERA5.1 data collection.

453 References

- 454 Allen, D. R., Bevilacqua, R. M., Nedoluha, G. E., Randall, C. E., and Manney, G. L.: Unusual stratospheric transport and
- 455 mixing during the 2002 Antarctic winter, Geophys. Res. Lett., 30, https://doi.org/10.1029/2003GL017117, 2003.
- 456 Andrews, D. G., Holton, J. R., and Leovy, C. B.: Middle Atmosphere Dynamics. Academic Press, San Diego, CA, 489 pp.,
- 457 ISBN 9780120585762, 1987.
- 458 Baldwin, M., Hirooka, T., O'Neill, A., Yoden, S: Major stratospheric warming in the Southern Hemisphere in 2002:
- 459 Dynamical aspects of the ozone hole split, SPARC Newsl., 20, 24–26, 2003.
- 460 Charlton, A. J., O'Neill, A., Lahoz, W. A., and Berrisford, P.: The splitting of the stratospheric polar vortex in the Southern
- 461 Hemisphere, September 2002: Dynamical evolution, J. Atmos. Sci., 62, 590–602, https://doi.org/10.1175/JAS-3318.1, 2005.
- 462 Charlton, A. J. and Polvani, L. M.: A new look at stratospheric sudden warmings. Part I: climatology and modeling
- 463 benchmarks, J. Climate, 20, 449–469, https://doi.org/10.1175/JCLI3996.1, 2007.
- 464 Charney, J. G. and Drazin, P. G.: Propagation of planetary-scale disturbances from the lower into the upper atmosphere, J.
- 465 Geophys. Res., 66, 83–109, https://doi.org/10.1029/JZ066i001p00083, 1961.
- 466 Gray, L., Norton, W., Pascoe, C., and Charlton, A.: A possible influence of equatorial winds on the September 2002
- 467 Southern Hemisphere sudden warming event, J. Atmos. Sci., 62, 651–667, https://doi.org/10.1175/JAS-3339.1, 2005.
- 468 Dickinson, R. E.: Baroclinic instability of an unbounded zonal shear flow in a compressible atmosphere, J. Atmos. Sci., 30,
- 469 1520–1527, https://doi.org/10.1175/1520-0469(1973)030<1520:BIOAUZ>2.0.CO;2, 1973.
- 470 Gelaro, R., McCarty, W., Suarez, M. J., Todling, R., Molod, A., Takacs, L., Randles, C. A., Darmenov, A., Bosilovich, M.
- 471 G., Reichle, R., Wargan, K., Coy, L., Cullather, R., Draper, C., Akella, S., Buchard, V., Conaty, A., da Silva, A. M., Gu, W.,
- 472 Kim, G.-K., Koster, R., Lucchesi, R., Merkova, D., Nielsen, J. E., Partyka, G., Pawson, S., Putman, W., Rienecker, M.,
- 473 Schubert, S. D., Sienkiewicz, M., and Zhao, B.: The Modern-Era Retrospective Analysis for Research and Applications,
- 474 Version 2 (MERRA-2), J. Climate, 30, 5419–5454, https://doi.org/10.1175/JCLI-D-16-0758.1, 2017.

- 475 Harnik, N. and Heifetz, E.: Relating overreflection and wave geometry to the counterpropagating Rossby wave perspective:
- 476 Toward a deeper mechanistic understanding of shear instability, J. Atmos. Sci., 64, 2238–2261,
- 477 https://doi.org/10.1175/JAS3944.1, 2007.
- 478 Holton, J. R. and Tan, H.-C.: The quasi-biennial oscillation in the Northern Hemisphere lower stratosphere, J. Meteorol. Soc.
- 479 Jpn., 60, 140–148, https://doi.org/10.2151/jmsj1965.60.1 140, 1982.
- 480 Iida, C., Hirooka, T., and Eguchi, N.: Circulation changes in the stratosphere and mesosphere during the stratospheric sudden
- 481 warming event in January 2009, J. Geophys. Res. Atmos., 119, 7104–7115, https://doi.org/10.1002/2013JD021252, 2014.
- 482 Jucker, M.: Scaling of Eliassen-Palm flux vectors, Atmos. Sci. Lett., 22, e1020, https://doi.org/10.1002/asl.1020, 2021.
- 483 Karoly, D. J. and Hoskins, B. J.: Three-dimensional propagation of planetary waves, J. Meteorol. Soc. Jpn., 60, 109–122,
- 484 https://doi.org/10.2151/jmsj1965.60.1 109, 1982.
- 485 Kosaka, Y., Kobayashi, S., Harada, Y., Kobayashi, C., Naoe, H., Yoshimoto, K., and Onogi, K.: The JRA-3Q reanalysis, J.
- 486 Meteorol. Soc. Jpn. Ser. II. 102, 49–109, https://doi.org/10.2151/jmsi.2024-004, 2024.
- 487 Koushik, N., Kumar, K. K., and Pramitha, M.: A tropical stratopause precursor for sudden stratospheric warmings, Sci. Rep.,
- 488 12, 2937, https://doi.org/10.1038/s41598-022-06864-7, 2022.
- 489 Krüger, K., Naujokat, B., and Labitzke, K.: The unusual midwinter warming in the Southern Hemisphere stratosphere 2002:
- 490 A comparison to Northern Hemisphere phenomena, J. Atmos. Sci., 62, 603–613, https://doi.org/10.1175/JAS-3316.1, 2005.
- 491 McFarlane, N. A.: The effect of orographically excited gravity wave drag on the general circulation of the lower stratosphere
- 492 and troposphere, J. Atmos. Sci., 44, 1775–1800, https://doi.org/10.1175/1520-0469(1987)044<1775:TEOOEG>2.0.CO;2,
- 493 1987.
- 494 Manney, G. L., Sabutis, J. L., Allen, D. R., Lahoz, W. A., Scaife, A. A., Randall, C. E., Pawson, S., Naujokat, B., and
- 495 Swinbank, R.: Simulations of dynamics and transport during the September 2002 Antarctic major warming, J. Atmos. Sci.,
- 496 62, 690–707, https://doi.org/10.1175/JAS-3313.1, 2005.
- 497 Matsuno, T.: Vertical propagation of stationary planetary waves in the winter Northern Hemisphere, J. Atmos. Sci., 27, 871–
- 498 883, https://doi.org/10.1175/1520-0469(1970)027<0871:VPOSPW>2.0.CO;2, 1970.
- 499 Matsuno, T.: A dynamical model of the stratospheric sudden warming, J. Atmos. Sci., 28, 1479–1494,
- 500 https://doi.org/10.1175/1520-0469(1971)028<1479:ADMOTS>2.0.CO;2, 1971.
- 501 McIntyre, M. E.: How well do we understand the dynamics of stratospheric warmings? J. Meteorol. Soc. Jpn. Ser. II, 60, 37–
- 502 65, https://doi.org/10.2151/jmsj1965.60.1 37, 1982.
- 503 Molod, A., Takacs, L., Suarez, M., and Bacmeister, J.: Development of the GEOS-5 atmospheric general circulation model:
- 504 Evolution from MERRA to MERRA-2, Geosci. Model Dev., 8, 1339–1356, https://doi.org/10.5194/gmd-8-1339-2015, 2015.
- 505 Newman, P. A. and Nash, E. R.: The unusual Southern Hemisphere stratosphere winter of 2002, J. Atmos. Sci., 62, 614–628,
- 506 https://doi.org/10.1175/JAS-3323.1, 2005.

- 507 O'Neill, A., Oatley, C. L., Charlton-Perez, A. J., Mitchell, D. M., and Jung, T.: Vortex splitting on a planetary scale in the
- 508 stratosphere by cyclogenesis on a subplanetary scale in the troposphere, O. J. R. Meteorol, Soc., 143, 691–705,
- 509 https://doi.org/10.1002/qj.2957, 2017.
- 510 Rhodes, C. T., Limpasuvan, V., and Orsolini, Y. J.: Eastward-propagating planetary waves prior to the January 2009 sudden
- 511 stratospheric warming, J. Geophys. Res. Atmos., 126, e2020JD033696, https://doi.org/10.1029/2020JD033696, 2021.
- 512 Rhodes, C. T., Limpasuvan, V., and Orsolini, Y.: The composite response of traveling planetary waves in the middle
- 513 atmosphere surrounding sudden stratospheric warmings through an overreflection perspective, J. Atmos. Sci., 80, 2635–2652,
- 514 <u>https://doi.org/10.1175/JAS-D-22-0266.1</u>, 2023.
- 515 Ryoo, J. M. and Chun, H. Y.: Stratospheric major sudden warmings revealed in NCEP reanalysis data for 41 years (1958-
- 516 1999), Asia-Pac. J. Atmos. Sci., 41, 173–190, 2005.
- 517 Salby, M. L. Fundamentals of Atmospheric Physics. Int. Geophys. Ser. 61, Academic Press, San Diego, CA, 648 pp., ISBN
- 518 9780080532158, 1996.

- 519 Simmons, A., Hersbach, H., Dee, D., and Berrisford, P.: Global stratospheric temperature bias and other stratospheric
- 520 aspects of ERA5 and ERA5.1, ECMWF Tech. Rep., https://doi.org/10.21957/rexqfmg0, 2020.
- 521 Song, B. G., Chun, H. Y., and Song, I. S.: Role of gravity waves in a vortex-split sudden stratospheric warming in January
- 522 2009, J. Atmos. Sci., 77, 3321–3342, https://doi.org/10.1175/JAS-D-20-0039.1, 2020.
- 523 Vallis, G. K.: Atmospheric and Oceanic Fluid Dynamics, Cambridge University Press, Cambridge, 2017.
- 524 Yoo, J. H., Chun, H. Y., and Kang, M. J.: Vortex preconditioning of the 2021 sudden stratospheric warming: Barotropic-
- 525 baroclinic instability associated with the double westerly jets, Atmos. Chem. Phys., 23, 10869-10881,
- 526 https://doi.org/10.5194/acp-23-10869-2023, 2023.
- 527 Yoo, J. H., Chun, H. Y., and Song, I. S.: In situ generation of planetary waves in the mesosphere by zonally asymmetric
- 528 gravity wave drag: A revisit, J. Atmos. Sci., 81, 1617–1639, https://doi.org/10.1175/JAS-D-24-0026.1, 2024.